

Biochemical relevance of Cr(III) complexes of isoniazid: Synthesis, characterization, DFT, antibacterial screening, antioxidant activity and glucose lowering effect in STZ-induced diabetic rats

Satyendra N. Shukla, Pratiksha Gaur, Sangeeta Jhariya, Bhaskar Chaurasia, Preeti Vaidya & M. Azam

To cite this article: Satyendra N. Shukla, Pratiksha Gaur, Sangeeta Jhariya, Bhaskar Chaurasia, Preeti Vaidya & M. Azam (2019): Biochemical relevance of Cr(III) complexes of isoniazid: Synthesis, characterization, DFT, antibacterial screening, antioxidant activity and glucose lowering effect in STZ-induced diabetic rats, Journal of Coordination Chemistry, DOI: [10.1080/00958972.2019.1572885](https://doi.org/10.1080/00958972.2019.1572885)

To link to this article: <https://doi.org/10.1080/00958972.2019.1572885>



View supplementary material [↗](#)



Accepted author version posted online: 25 Jan 2019.



Submit your article to this journal [↗](#)



View Crossmark data [↗](#)

Biochemical relevance of Cr(III) complexes of isoniazid: Synthesis, characterization, DFT, antibacterial screening, antioxidant activity and glucose lowering effect in STZ-induced diabetic rats

SATYENDRA N. SHUKLA*[†], PRATIKSHA GAUR[†], SANGEETA JHARIYA[†], BHASKAR CHAURASIA[†], PREETI VAIDYA[†] and M. AZAM[‡]

[†]Coordination Chemistry Research Lab, Department of Chemistry, Govt. Science College, Jabalpur (M.P.) India

[‡]King Saud University, Riyadh, Saudi Arabia

Molecular mechanism suggests that the incorporation of an antioxidant organic moiety to chromium will be a sound strategy for the synthesis of safer and more effective hypoglycemic compounds. Two Schiff base ligands were derived by condensation of isonicotinyl hydrazide with salicylaldehyde/*o*-hydroxyacetophenone which further yield four novel chromium(III) complexes of types $[\text{Cr}(\text{L})\text{Cl}_2(\text{H}_2\text{O})]$ and $[\text{Cr}(\text{L})_2]\text{Cl}$. The ligands and complexes were characterized by analytical and spectroscopic techniques. DFT study at the basic set B3LYP and TD-SCF/6-311-G level was employed to confirm the geometry of the investigated compounds. Ligands were tested for their antioxidant activity and exhibited good antioxidant activity. Assessment of insulin-like activity of the complexes was initially performed *in vitro* by measuring the inhibition of α -amylase. The complex with highest *in vitro* activity was investigated for *in vivo* antidiabetic activity on the model of STZ-induced diabetic rats, which demonstrated that complex 4 significantly lowers the blood glucose level in rats. Toxicity level and antioxidant activity of the complex were also tested, which exhibit good tolerance level and antioxidant activity. Histological analysis of the pancreas of animals under investigation reveals the good condition of the pancreas treated with the complex. Ligands and complexes were also tested for antibacterial activity against *E. coli*.

Keywords: α -Amylase inhibition; Schiff base; Type-2 diabetes mellitus; *In vivo* activity; DFT

1. Introduction

Diabetes, particularly type II diabetes, is a very severe disease affecting the health of the human being worldwide, making it one of the most important public health challenges to all countries.

*Corresponding author. Emails: ccr1_2004@rediffmail.com; sns1963_1@rediffmail.com

There are reports indicating the estimation of affected people may be 349 million by 2025 [1]. Diabetes Mellitus is a disease that results in chronic hyperglycemia due to an absolute or relative lack of insulin and insulin resistance which in turn impairs the metabolism of glucose [2, 3]. Over the years, various antidiabetic drugs with main products metformin, DPP-4 inhibitors, GLP-1 receptor agonists, pioglitazone glucosidase inhibitors, sulfonylureas/glinides, acarbose, and SGLT-2 inhibitors are available on the market [4]. The digestive enzyme pancreatic α -amylase (EC 3.2.1.1) is a calcium metalloenzyme that catalyzes the hydrolysis of the α -1,4-glycosidic linkages of the starch, amylose, amylopectin, glycogen and various maltodextrins, and is responsible for most of the starch digestion in humans. In this context, it is important to mention that the inhibition of carbohydrate digestive enzyme α -amylase that plays an important role in the digestion of starch and glycogen is considered an important therapeutic strategy for the treatment of type II diabetes and obesity as well as dental caries and periodontal disease [5].

Metal-containing compounds have been used in medicine since long [6]. Chromium is considered an essentially important metal for normal glucose and lipid homeostasis [7]. Chromium picolinate and picolinic acid are the most extensively studied as antidiabetic and antiobesity chromium complex [8]. Furthermore, Cr(III) ion plays a valuable role in the regulation of insulin action, metabolic syndrome and cardiovascular disease, and facilitates the interaction of insulin with its receptor on the cell surface [9-12].

Isonicotinyl hydrazide or isoniazid is an antibacterial compound, very active on the bacterial strain *M. tuberculosis*, *M. bovis* and *M. canis* [13]. It is highly specific and surprisingly effective against other microorganisms and so it is now a frontline drug used in antitubercular treatment (ATT) [14]. Schiff bases and their metal complexes are known to have biological activities such as antifungal, antimicrobial, antitumor, antioxidant, antidiabetic and herbicidal properties [15-23]. They have also been widely used as versatile ligands involved in various metal chelation reactions to form metal complexes which are very interesting in many fields, such as catalysis, enzymatic reactions and antioxidant activity.

Molecular mechanism suggests that a synergistic combination of antioxidant organic ligands with chromium will be a sound strategy for the synthesis of safer and more effective hypoglycemic compounds [24-26]. Thus, in view of these significant biological activities of isoniazid as well as the biomimetic activity of chromium, we have started the work with the aim to synthesize complexes of Schiff bases derived from isoniazid with

salicylaldehyde/*o*-hydroxyacetophenone in anticipation of a good antidiabetic and antioxidant activity. In addition, mole ratios for the reactions are determined by spectral measurements. Stability constants (K) and Gibbs free energy (ΔG) values were also calculated. We are also interested in the antidiabetic activity of resulting complexes with *in vitro* and *in vivo* experimental systems in order to explore their effectiveness. We have used density functional theory (DFT) calculations to ascertain the molecular structure of the ligands and complexes.

2. Experimental

2.1. Chemicals and techniques

All the chemicals and solvents were used of A.R. grade. Chromium(III) chloride hexahydrate was purchased from Research Lab and used without purification. Solvent methanol and ethanol (E. Merck) were distilled before use. Chromium was determined gravimetrically [27]. Isonicotinyl hydrazide (Lancaster, U.K.), salicylaldehyde (E. Merck) and *o*-hydroxyacetophenone (CDH) were used as received. Enzyme alpha-amylase was purchased from Himedia, streptozotocin (Sigma Aldrich, Germany). FTIR spectra were recorded on a Shimadzu-8400 S FTIR spectrophotometer in the range 4000-400 cm^{-1} . Electronic spectra were measured on an EI-2305 UV-vis spectrophotometer in DMSO- d_6 . $^1\text{H-NMR}$ and $^2\text{D-NMR}$ spectra (HSQC) were recorded in DMSO- d_6 on an Agilent-700-vnmrs700 spectrophotometer. The ESI-MS spectra were recorded on an Agilent 6520 (QTOF) mass spectrometer having a DART source in methanol. Elemental analyses (C, H, and N) were performed on an Elementar Vario EL III, Elemental Analyzer. Gouy's method was employed for measurement of magnetic susceptibility; $\text{Hg}[\text{Co}(\text{NCS})_4]$ was used as a standard. Diamagnetic correction was made using Pascal's constants. Molar conductance was measured in DMSO with an EI-181 digital conductivity bridge using a dipping type of cell at 25 $^\circ\text{C}$ [28]. Glucose levels were estimated by Glucometer (Accu check Performa).

2.2. Synthesis of Schiff base ligands

2.2.1. Preparation of (E)-N'-(2-hydroxybenzylidene)isonicotinohydrazide (L_1).

Salicylaldehyde (1.06 mL, 0.01 mol) dissolved in ethanol was added to a solution of isonicotinyl hydrazide (1.37 g, 0.01 mol) in ethanol and the reaction mixture was stirred for 1 h. Thereafter, it was refluxed for 12 h. Progress of the reaction was observed by TLC. After completion, the

reaction mixture was concentrated to one-fourth of its volume and cooled to room temperature. After two days of slow evaporation, a cream-white precipitate was separated, which was filtered off, washed with sodium bisulphate, vacuum dried and recrystallized from 1:1 ethanol:water mixture (v/v). Color: cream white; Yield: 2.14 g (89.00%); m.p. = 221 °C; Found: C, 64.60; H, 4.60; N, 17.36 %; $C_{13}H_{11}N_3O_2$ (MW = 241.25) requires: C, 64.66; H, 4.61; N, 17.40 %. Selected IR absorptions (KBr, cm^{-1}): $\nu(O-H)$, 3350(w); $\nu(N-H)$, 3194(w); $\nu(CO)_{CONH}$, 1681(s); $\nu(C=N)_{cyclic} + \nu(HC=N)_{imine}$, 1618(s). Electronic spectra (λ_{max} , in nm (ϵ , in $M^{-1}cm^{-1}$)) in DMSO: 220(310), 250(215), 300(120). ^1H-NMR (700 MHz; δ , DMSO- d_6), δ (ppm): 13.285 (s, 1H, -OH); 11.678 (s, 1H, -CONH); 8.512 (s, 1H, -CH=N); 8.456 (d, J = 5.4 Hz, 2H, pyridyl); 7.911 (d, J = 5.4 Hz, 2H, pyridyl); 7.316 (s, 1H, aromatic); 7.214 (d, J = 7.3 Hz, 2H, aromatic); 6.922 (dd, J = 9.5, 4.6 Hz, 1H, aromatic). ESI-mass spectra, m/z: $[C_6H_4NO]^+ = 106.03$, $[C_7H_6NO]^+ = 120.04$, $[C_6H_5N_2O]^+ = 121.04$, $[C_7H_7N_2O]^+ = 135.05$, $[C_7H_6N_3O]^+ = 148.05$, $[C_8H_7N_2O_2]^+ = 163.05$, $[C_{13}H_{10}N_3O]^+ = 224.08$, $[C_{13}H_{10}N_3O_2]^+ = 240.08$, $[C_{13}H_{11}N_3O_2 + H^+]^+ = 242.04$, MW = 241.09.

2.2.2. Preparation of (E)-N-(1-(2-hydroxyphenyl) ethylidene)isonicotinohydrazide (L₂).

Isonicotinyl hydrazide (1.37 g, 0.01 mol) dissolved in ethanol was mixed with *o*-hydroxyacetophenone (1.20 mL, 0.01 mol) in ethanol and the reaction mixture was stirred for 2 h. Thereafter, it was refluxed for 15 h. Progress of the reaction was observed by TLC. After completion, the reaction mixture was concentrated and cooled to room temperature. After slow evaporation, a white precipitate was obtained, which was filtered off, washed with sodium bisulphate, vacuum dried and recrystallized from DMSO. Color: white; Yield: 2.066 g (81.00%); m.p. = 218 °C. Found: C, 64.70; H, 5.08; N, 16.28 %; $C_{14}H_{13}N_3O_2$ (MW = 255.10) requires: C, 64.75; H, 5.10; N, 16.39 %; Selected IR absorptions (KBr, cm^{-1}): $\nu(O-H)$, 3352(w); $\nu(N-H)$, 3120(w); $\nu(CO)_{CONH}$, 1680(s); $\nu(C=N)_{cyclic} + \nu(HC=N)$, 1610(s). Electronic spectra (λ_{max} , in nm (ϵ , in $M^{-1}cm^{-1}$)) in DMSO: 220(318), 250(225), 300(125). ^1H-NMR (700 MHz; δ , DMSO- d_6), δ (ppm): 13.188 (s, 1H, -OH); 11.589 (s, 1H, -CONH); 8.785 (d, J = 5.6 Hz, 2H, pyridyl); 7.837 (d, J = 5.5 Hz, 2H, pyridyl); 7.316 (s, 1H, aromatic); 7.646 (d, J = 7.7 Hz 2H, aromatic); 6.914 (dd, J = 9.8, 4.9 Hz, 1H, aromatic); 2.493 (s, 3H, methyl). ESI-mass spectra, m/z: $[C_{14}H_{13}N_3O_2 + H^+]^+ = 256.1$; $[C_{14}H_{13}O_2N_2^{15}N + H^+]^+ = 257.10$, MW = 255.10.

2.3. Synthesis of complexes

2.3.1. Complex [Cr(L₁)Cl₂(H₂O)] (1). To the solution of chromium(III) chloride (0.266 g, 1.0 mmol) in ethanol, recrystallized Schiff base ligand L₁ (0.241 g, 1.0 mmol) dissolved in hot ethanol was added. A few drops of sodium hydroxide were added which works as a catalyst, and the reaction mixture was kept under stirring for 2 h in an inert atmosphere. The color of the reaction mixture changed from dark yellow to brown. Thereafter, the reaction mixture was refluxed for 12 h. After reduction of volume by slow evaporation, a brown solid was precipitated in each case, which was filtered off, washed with acetone, dried under vacuum and recrystallized from ethanol. Color: brown; Yield: 0.453 g (89%); m.p. = 250 °C. Found: C, 42.20; H, 3.80; N, 10.55; Cr, 12.95 %; C₁₄H₁₅Cl₂CrN₃O₃ (MW = 396.19) requires: C, 42.44; H, 3.82; N, 10.61; Cr, 13.12 %. Selected IR absorptions (KBr, cm⁻¹): ν(N-H), 3201(w); ν(C=O), 1642(s); ν(C=N)_{cyclic}+ν(C=N), 1600(s), 1570(s); δ(H₂O), 771(s); ν(M-N), 750(m); ν(M-O), 428(m). Electronic spectra (λ_{max}, in nm (ε, in M⁻¹cm⁻¹)) in DMSO: 290(252), 320(180), 335(90), 440(20), 520(18). μ_{eff} = 3.80 BM. Molar conductance in DMSO-d₆, Λ_m at 25 °C (Ω⁻¹cm²mol⁻¹) = 3. ESI-mass spectra, m/z: [Cl₂CrH₂O]⁺ = 139.89; [C₁₄H₁₃N₃O₂ + 2H]⁺ = 257.10; [C₁₄H₁₅ClCrN₃O₃]⁺ = 342.01; [C₁₄H₁₅Cl₂CrN₃O₃ + H⁺]⁺ = 395.98 (MW = 396.19).

2.3.2. Complex [Cr(L₁)₂]Cl (2). Chromium(III) chloride (0.266 g, 1.0 mmol) dissolved in 20 mL ethanol was mixed with an ethanolic solution of recrystallized Schiff base ligand L₁ (0.482 g, 2.0 mmol). A few drops of sodium hydroxide were added, and the reaction mixture was kept under stirring for 3 h in an inert atmosphere. The color of the reaction mixture changed from dark yellow to brown. Thereafter, the reaction mixture was refluxed for 14 h. After reduction of volume by slow evaporation a red-brown solid was precipitated, which was filtered off, washed with acetone, dried under vacuum and recrystallized from ethanol. Color: red-brown; Yield: 0.641 g (85%); m.p. = 240 °C; Found: C, 54.70; H, 3.50; N, 14.60; Cr, 8.95 %; C₂₆H₂₀Cl₃CrN₆O₄ (MW = 567.92) requires: C, 54.99; H, 3.55; N, 14.80; Cr, 9.16 %. Selected IR absorptions (KBr, cm⁻¹): ν(N-H), 3053(w); ν(C=O), 1630(s); ν(C=N), 1602(s); ν(M-O), (766); ν(M-O), 464(m). Electronic spectra (λ_{max}, in nm (ε, in M⁻¹cm⁻¹)) in DMSO: 295(320), 324(204), 330(94), 430(18), 515(22). μ_{eff} = 3.65 BM. Molar conductance in DMSO-d₆, Λ_m at 25 °C (Ω⁻¹cm²mol⁻¹) = 49. ESI-mass spectra, m/z: [C₁₃H₁₀N₃O₂ + 2H⁺] = 242.08; [C₁₉H₁₄CrN₃O₃]⁺ = 384.33; [C₂₁H₁₆CrN₅O₄]⁺ = 454.06; [C₂₆H₂₀CrN₆O₄]⁺ = 532.10 (MW = 567.90).

2.3.3. Complex [Cr(L₂)(Cl₂)(H₂O)] (3). Chromium(III) chloride (0.266 g, 1.0 mmol) completely dissolved in 20 mL of ethanol was mixed with 20 mL solution of recrystallized Schiff base ligand L₂ (0.255 g, 1.0 mmol) in ethanol. A few drops of sodium hydroxide were added, and the reaction mixture was kept under stirring for 2 h in an inert atmosphere. The color of the reaction mixture changed from dark yellow to brown. Thereafter, the reaction mixture was refluxed for 15 h. After reduction of volume by slow evaporation a solid was precipitated, which was filtered off, washed with acetone, dried under vacuum and recrystallized from methanol:carbon tetrachloride 1:2 (v/v). Color: brown; Yield: 0.501g (95%); m.p. = 250 °C; Found: C, 43.80; H, 4.15; N, 10.20; Cr, 12.50 %; C₁₅H₁₅Cl₃CrN₃O₂ (MW = 410.22) requires: C, 43.92; H, 4.18; N, 10.24; Cr, 12.68 %. Selected IR absorptions (KBr, cm⁻¹): ν(N-H), 3155(w); ν(C=O), 1640(s); ν(C=N), 1604(s), 1580(s); δ(H₂O), 778(s); ν(M-N), 755(m); ν(M-O), 430(m). Electronic spectra (λ_{max}, in nm (ε, in M⁻¹cm⁻¹)) in DMSO: 290(320), 320(204), 330(94), 438(28), 525(20). μ_{eff} = 3.70 BM. Molar conductance in DMSO-d₆, Λ_m at 25 °C (Ω⁻¹ cm²mol⁻¹) = 5. ESI-mass spectra, m/z: [C₁₅H₁₅N₃O₂ + 2H⁺] = 269.10; [C₁₀H₁₁Cl₃CrN₂O₂]⁺ = 347.93; [C₁₅H₁₅Cl₂CrN₃O₂]⁺ = 390.99; [C₁₅H₁₅Cl₃CrN₃O₂ + H⁺]⁺ = 409.96 (MW = 410.22).

2.3.4. Complex [Cr(L₂)₂]Cl (4). Chromium(III) chloride (0.266 g, 1.0 mmol) completely dissolved in methanol and 20 mL of ethanol was mixed with a solution of recrystallized Schiff base ligand L₂ (0.51 g, 2.0 mmol) with the same solvent. A few drops of sodium hydroxide were added, and the reaction mixture was kept under stirring for 4 h in an inert atmosphere. The color of the reaction mixture changed from dark yellow to brown. Thereafter, the reaction mixture was refluxed for 16 h. After reduction of volume by slow evaporation a brown solid was precipitated, which was filtered off, washed with acetone, dried under vacuum and recrystallized from methanol:chloroform 1:2 (v/v). Color: pale brown; Yield: 0.620g (79%); m.p. = 280 °C; Found: C, 55.80; H, 4.01; N, 14.05; Cr, 8.40 %; C₂₈H₂₄ClCrN₆O₄ (MW = 595.98) requires: C, 56.43; H, 4.06; N, 14.10; Cr, 8.72%. Selected IR absorptions (KBr, cm⁻¹): ν(N-H), 3066(w); ν(C=O), 1633(s); ν(C=N), 1590(s), 1573(s); ν(M-N), 576(m); ν(M-O), 426(m). Electronic spectra (λ_{max}, in nm (ε, in M⁻¹cm⁻¹)) in DMSO: 260(320), 280(204), 340(94), 380(18), 420(26). μ_{eff} = 3.73 BM. Molar conductance in DMSO-d₆, Λ_m at 25 °C (Ω⁻¹ cm² mol⁻¹) = 54. ¹H-NMR (700 MHz; DMSO-d₆), δ (ppm): 11.489 (s, 2H, -CONH); 8.710 (d, 2H, pyridyl), 7.316 (m, 8H, Ar-H); 6.002

(m, 4H, Ar-H); 2.487 (s, 6H, -CH₃). ESI-mass spectra, m/z: [C₁₄H₁₂N₆O₄ + 2H⁺] = 256.10; [C₂₈H₂₄CrN₆O₄]⁺ = 560.13 (MW = 595.10).

2.4. Stability parameters

Job's method [29] was employed to determine the stoichiometric ratio and stability constant (K) of the complexes [30]. The solutions were prepared by mixing solutions of both ligand and metal salt with equal molar concentration (10⁻³ M in DMSO) in ratio varying from 1:9 to 9:1. The absorbance was measured at 465 nm for complex **1**, 475 nm for complex **2**, 460 nm for complex **3** and 455 nm for complex **4**.

Preferably, only the complex species stable in solution ML_n have absorbance under a monochromatic light at the definite wavelength. The mole fraction change as increases from 0 to 1, the absorbance of solution system first increases and decreases afterwards. These changes are plotted as absorbance *versus* f graph known as Job's curve. With the help of the graph, we can get the coordination number "n" by eq. 1:

$$n = 1 - f/f_0 \quad (1)$$

where f is molar concentration of metal ion and ligand and calculated by eq. 2.

$$f = [M] / ([M] + [L]) \quad (2)$$

The degree of dissociation α is calculated by Job's curve by the following formula (eq. 3).

$$\alpha = (A - A_0) / A \quad (3)$$

The stability constant (K) and degree of dissociation (α) of complexes are calculated by equation 4:

$$K = \frac{1 - \alpha}{n^n [M]^n \alpha^{n+1}} \quad (4)$$

where M is a concentration of metal ion, α is degree of dissociation of complex and n is coordination number of complex.

2.5. Computational analysis

In order to understand the molecular structure of the ligands and complexes, we have done DFT calculations using Gaussian 09 software package [31]. DFT calculations were performed by full-geometry optimization of the ligands and complexes **1-4** by using DFT method of B3LYP with 6-311+G(d, 2p) and/or 3-21+G* basis set for all nonmetallic atoms and LANL2DZ basis set for the central metal atoms in the gas phase [32]. The quantum chemical parameters such as E_{HOMO} , E_{LUMO} , Mulliken electronegativity (χ), dipole moment, chemical potential (P_i), global hardness (η), global softness (S), global electrophilicity (ω), absolute softness (σ), electronic charge (ΔN_{max}) and total energy (ETD-HF/ETDKS) were calculated after geometrical optimization of the structure of all compounds. The optimized structural parameters such as bond lengths, bond angles and dihedral angles of all the compounds were determined with the atom numbering scheme of the molecule. The distribution of electronegativity/electropositivity over a large number of atoms was presented by the molecular electrostatic potential (MEP) [33].

2.6. Biological studies

2.6.1. *In vitro* antioxidant assay (DPPH free radical scavenging activity) of ligands. The free radical scavenging activity of ligands was determined with the 2,2-diphenyl-1-picrylhydrazyl (DPPH) method. Four solutions of different micromolar concentrations of compounds (0.002 μM , 0.004 μM , 0.006 μM and 0.008 μM) and standard ascorbic acid were prepared in ethanol. The volume of each test tube was adjusted to 1.0 mL by adding ethanol. DPPH was used as a control. Thereafter, 5 mL ethanolic solution of DPPH (0.1 mM) was added. The tubes were kept at ambient temperature for 30 min. The absorbance of test solutions and a blank solution of DPPH (2 mL) was measured at 517 nm. The decrease in the absorbance of DPPH was calculated comparative to the measured absorbance of the control [34]. The percentage of radical scavenging activity was calculated using the following formula:

$$\% \text{ Radical scavenging activity} = \frac{\text{Absorbance of control} - \text{Absorbance of the test}}{\text{Absorbance of control}} \times 100$$

2.6.2. Antidiabetic activity

2.6.2.1. *In vitro* antidiabetic activity of complexes

This study was performed by a modified starch iodine protocol [35]. In short, 0.01 mL of each compound solution (0.002 μ M in DMSO) was taken in pre-labelled test tubes. The enzyme solution was prepared by mixing 27.5 mg of α -amylase in 100 mL of distilled water. After that, 0.02 mL of α -amylase was added to each test tube and incubated for 10 min at 37 °C. After incubation, 2 mL acetate buffer was added to each test tube, thereafter, 0.2 mL of 1% starch solution was added to each test tube and the mixture was reincubated for 1 h at 37 °C. Then 0.2 mL of 1% iodine solution was added to each test tube. The absorbance of the mixture was taken at 565 nm. Sample, substrate and α -amylase blank were undertaken under the same conditions. Each experiment was done in triplicate. Percent α -amylase inhibition was determined by the following equation:

$$\% \alpha \text{ amylase inhibition} = \frac{\text{Absorbance of control} - \text{Absorbance of the test}}{\text{Absorbance of control}} \times 100$$

2.6.2.2. *In vivo* antidiabetic activity of complex

Complex **4** was one of the most active in the *in vitro* experiment, which was selected for *in vivo* antidiabetic activity. Healthy male *Albino wistar* rats weighing 200 \pm 30 g were used for all experiments in the present study. Rats were housed in polycarbonate cages in a group of three animals provided with husk bedding. All animals were kept at 22 \pm 2 °C in 12:12 h, light:dark cycle. Feeding was done with standard pellets diet supplied by Golden Feeds, New Delhi (India); drinking allowed with purified water *ad libitum*. Animals were collected at random from Animal house of PBRI, Bhopal (India). All animal experiments were approved by the Institutional Animal Ethics Committee (IAEC) of PBRI, Bhopal (CPCSEA Reg. No.1824/PO/ERe/S/15/CPCSEA). Protocol approval reference no. PBRI/IAEC/PN-17031.

2.6.2.2.1. *Induction of diabetes*. Animals (*Albino wistar*) were kept for overnight fasting by depriving of food for 16 h but allowed free access to water. Streptozotocin was dissolved in citrate buffer (pH 4.5) and nicotinamide, in normal physiological saline. Non-insulin dependent diabetes mellitus was induced in overnight fasting rats by a single intraperitoneal injection of 60 mg/kg streptozotocin. After 15 min i.p. administration, 120 mg/kg of nicotinamide was

injected. Hyperglycemia confirmed by the elevated levels of blood glucose were determined at 72 h. Only rats confirmed to have permanent NIDDM (non-insulin dependent diabetes mellitus) were used for the antidiabetic study [36]. The animals with blood glucose concentration more than 250 mg/dL will be used for the study.

2.6.2.2.2. *Acute oral toxicity.* Acute oral toxicity test was performed according to OECD guideline 423. Present study was conducted for the evaluation of acute toxicity study of the complex in *Albino wistar* rat. General behavior and lethality were evaluated and toxicity was observed through the dosing schedule of 14 days in 2000 mg/kg dose level groups.

2.6.2.2.3. *Experimental design.* The experimental design was modified from several previous works [37, 38]. All animals were divided randomly into five groups with three animals in each group. To the group first, received normal saline per oral only and served as vehicle control, the group second, third, fourth, and fifth were made diabetic with streptozotocin (STZ) and nicotinamide. Group second received saline, group third received glibenclamide tablet (600 µg/kg per day per oral) at the frequency of 24 h. Group fourth and fifth diabetic animals were administered orally 100 and 200 mg/kg chromium complex, respectively, daily for 21 days. All dosing of test samples was done orally throughout the experimentation. Test groups and their dosage levels are given in table S₁ in the Supplementary Material.

2.6.2.2.4. *Collection of blood samples.* After the last day of drug treatment, the blood sample was collected by a retro-orbital puncture at 0, 7, 14 and 21 days; the glucose levels were estimated by Glucometer (Accu check Performa). On day 21, oxidative enzyme (SOD, GSH, LPO and Catalase) also estimated in blood serum. Overall assessment of *in vivo* antidiabetic activity was shown as % glucose lowering (% GL):

$$\% \text{ GL} = \frac{(\text{glucose})\text{before treatment} - (\text{glucose})\text{after treatment}}{\text{glucose before treatment}} \times 100$$

2.6.2.2.5. *Statistical analyses.* All experimental results are expressed as the mean ± standard deviation (SD). All statistical data were analyzed with one-way analysis of variance (ANOVA)

followed by Bonferroni test. Differences resulting in P values < 0.05 were considered as the level of significance.

2.6.2.2.6. Histopathological examination of the pancreas. For dissection of the pancreas, a laparotomy was performed and the pancreas was immediately isolated and fixed overnight in 4% paraformaldehyde solution [39]. Cross sections of 4- μ m were cut and processed for routine staining with hematoxylin and eosin (H&E) and were used for histopathological examination under a light microscope (OPTICA). Photographs were then captured and diameters of ten random islets of Langerhans in each section were determined using GIMP 2.8.14 software. Diameters were then averaged for each animal and compared to determine the effect of drugs on the diseased islets.

2.6.3. Determination of oxidative enzyme levels

2.6.3.1. Preparation of tissue for assay

The organ was rinsed with ice-cold normal saline followed by 0.15 M HCl (pH 7.4). Thereafter, for LPO 10% w/v tissue homogenate in 0.15 M HCl (pH 7.4) and for GSH 10% w/v in 0.1 M phosphate buffer (pH 7.4) was taken as sample. However, for Catalase and SOD 10% w/v in 0.15 M HCl / 0.1 M phosphate buffer (pH 7.4) was used. The sample was centrifuged at 15,000 rpm for 15 min at 4 °C and supernatant were taken as a sample.

2.6.3.2. Determination of LPO level

To 0.2 mL of prepared tissue homogenate, 0.2 mL of 4% sodium dodecyl sulphate, 1.5 mL of 20% acetic acid and 1.5 mL of 0.5% thiobarbituric acid was added. The mixture was heated for 60 min at 95 °C in a temperature controlled water bath to give a pink color. The mixture was centrifuged at 3500 rpm for 10 min [40]. The absorbance of the supernatant was read spectrophotometrically at 532 nm.

2.6.3.3. Determination of GSH level

To 1 mL of tissue homogenate, 1 mL of 10% TCA was added. The precipitated fraction was centrifuged and to 0.5 mL supernatant, 2 mL of DTNB reagent was added. The final volume was made up to 3 mL with phosphate buffer. The color developed was read at 412 nm. A standard

curve for GSH was prepared using glutathione. Results were expressed as micromole of GSH/mg tissue [41].

2.6.3.4. Determination of CAT level

CAT level was estimated by the continuous spectrophotometric rate determination method [42]. A 50 μ L supernatant was added to the buffered substrate (50 mM phosphate buffer, pH 7 containing 10 mM H_2O_2) to make total volume 3 mL. The decrease in the absorbance was read at 240 nm for 2.5 min at an interval of 15 sec. The activity was calculated using extinction coefficient of H_2O_2 0.041/moles/cm². Results were expressed as moles of H_2O_2 utilized/min/mg protein.

2.6.3.5. Determination of SOD level

The assay involves the production of superoxide from O_2 using reduced b-nicotinamide adenine dinucleotide (NADH) as a reductant and phenazine methosulphate (PMS) as a catalyst in the presence of an indicator, nitro-blue tetrazolium (NBT), which turns blue when reduced by superoxide. The color change was monitored spectrophotometrically in the visible range at 560 nm. When aliquots of common beverages are added to the reaction, superoxide scavengers (*i.e.* antioxidants) compete with NBT to react with superoxide. The percent inhibition of NBT reduction can be used to quantify superoxide-scavenging [43, 44].

2.6.4. Antibacterial screening. Complexes **1-4** and ligands L_1 and L_2 were screened for antibacterial activity against gram-negative bacteria *E. coli* at different concentrations. Agar well diffusion method was used for antibacterial screening [45].

3. Results and discussion

3.1. Characterization of ligands

Empirical formulas of Schiff base ligands L_1 and L_2 were in agreement with elemental analysis. ESI-mass spectra of L_1 and L_2 exhibit several peaks depending on the fragmentation pattern and a molecular ion/pseudo-molecular ion peak [46]. L_1 shows peaks at m/z : 106.03, 120.04, 135.05, 224.08 and 242.04 attributed for $[\text{C}_6\text{H}_4\text{NO}]^+$, $[\text{C}_7\text{H}_6\text{NO}]^+$, $[\text{C}_7\text{H}_7\text{N}_2\text{O}]^+$ and $[\text{C}_{13}\text{H}_{11}\text{N}_3\text{O}_2+\text{H}^+]^+$, respectively. A peak at 242.04 was attributed to the pseudo-molecular ion. ESI-MS spectra of L_2

(figure S1 in the Supplementary Material) shows peaks at m/z : 256.10, 257.10 attributed for pseudo-molecular ion $[C_{14}H_{13}N_3O_2 + H^+]^+$ and its isotope $[C_{14}H_{13}O_2^{14}N_2^{15}N + H^+]^+$.

FT-IR spectra of L_1 and L_2 show absorption bands at 1618 cm^{-1} and 1610 cm^{-1} , respectively, which may be assigned for the combination of $\nu(C=N)_{\text{cyclic}}$ and $\nu(C=N)_{\text{imine}}$ [47]. However, both ligands exhibit a weak band at about 3350 cm^{-1} assigned for $\nu(O-H)$ vibration. A signal at $\sim 1681\text{ cm}^{-1}$ was assigned to $\nu(C=O)$ of CONH moiety. For ligands, theoretical IR spectra were elucidated with the help of DFT, which show a close resemblance with experimental FT-IR data. Theoretical IR spectrum of L_2 is shown in figure S2. However, FT-IR spectra of ligand L_2 and complex **4** are shown in figure S3.

The electronic spectra of Schiff base ligands exhibit three bands at $\sim 220\text{ nm}$, 260 nm and 300 nm . The first band was assigned to the $\pi-\pi^*$ transition of the C=C chromophore, however, the other two bands are assigned to $n-\pi^*$ transition associated with C=N and C=O groups, respectively. The UV-vis spectrum of L_2 is given in figure S4.

$^1\text{H-NMR}$ spectrum of L_1 exhibits a signal at 8.512 ppm assigned for one azomethine proton. Both L_1 and L_2 displayed a signal at 13.285 ppm and 13.188 ppm for one proton, each attributed to phenolic-OH. The signals observed at 11.678 ppm in L_1 and 11.589 ppm in L_2 for one proton each were assigned to (CO-NH) proton. L_2 shows a signal centered at 3.366 ppm for 3H was assigned for $-\text{CH}_3$ proton. In L_1 , two doublets centered at 8.456 ppm and 7.919 ppm for two protons were assigned to pyridyl protons. A singlet observed at 7.316 ppm for one proton, another doublet at 7.214 ppm for two protons and a triplet centered at 6.922 ppm were assigned to aromatic protons of the phenolic ring.

However, L_2 exhibits two doublets centered at 8.785 ppm and 7.845 ppm for two protons each assigned to pyridyl proton. A doublet centered at 7.316 ppm for one proton, another doublet at 7.646 ppm for one proton and a double doublet centered at 6.914 ppm for 2H were assigned to aromatic protons of the phenolic ring. $^1\text{H-NMR}$ spectrum of L_2 is shown in figure S5.

L_2 was also studied by 2D-HSQC spectrum (figure S6) which actually shows the connectivity of protons with different carbon atoms [48]. The two contours observed at 6.914 ppm were connected to phenolic carbon at 118 ppm and 119 ppm . The contours observed at 7.314 ppm and 7.646 ppm were connected with carbons at 132 ppm and 128 ppm . The contours observed at 7.845 and 8.780 ppm were connected with pyridyl carbons at 122.0 ppm and 149.0 ppm .

On the basis of the elemental analysis, ESI-MS, electronic, FT-IR and $^1\text{H-NMR}$ spectra, the following structures of L_1 and L_2 were proposed (figure 1).

3.2. Characterization of the complexes

The results of the elemental analysis of the metal complexes were in close agreement with the proposed chemical formula for the complexes. Molar conductance (Λ_m) of all complexes in 10^{-3} M in DMSO at 25°C was also helpful in proposing their formula. Molar conductance of complexes **1** and **3** is between $3\text{-}5\ \Omega^{-1}\text{cm}^2\text{mol}^{-1}$ indicating their non-ionic nature, however, **2** and **4** exhibit molar conductance of 49 and $54\ \Omega^{-1}\text{cm}^2\text{mol}^{-1}$ indicating 1:1 electrolytic nature in DMSO solution [49]. These complexes have shown the presence of Cl^- outside the coordination sphere by positive qualitative silver nitrate test. The structure of these complexes was also supported by ESI-MS.

ESI-mass spectra of the four complexes exhibit several peaks depending upon the fragmentation pattern including a molecular ion, M^+ or pseudo-molecular ion, $[\text{M} + \text{H}^+]^+$ peak [50]. Complex **1** shows peaks at m/z 139.89, 257.10, 342.01, 342.01, and 395.98 attributed to $[\text{C}_{14}\text{H}_{13}\text{N}_3\text{O}_2 + 2\text{H}]^+$, $[\text{C}_{14}\text{H}_{15}\text{ClCrN}_3\text{O}_3]^+$, $[\text{C}_{14}\text{H}_{15}\text{ClCrN}_3\text{O}_3]^+$, and $[\text{C}_{14}\text{H}_{15}\text{Cl}_2\text{CrN}_3\text{O}_3 + \text{H}^+]^+$, respectively. The peak at m/z 395.98 was a pseudo-molecular ion peak. In complex **2**, peaks appeared at m/z 242.08, 384.33, 454.06 and 532.10 attributed to $[\text{C}_{13}\text{H}_{10}\text{N}_3\text{O}_2 + 2\text{H}^+]^+$, $[\text{C}_{19}\text{H}_{14}\text{CrN}_3\text{O}_3]^+$, $[\text{C}_{21}\text{H}_{16}\text{CrN}_5\text{O}_4]^+$ and $[\text{C}_{26}\text{H}_{20}\text{CrN}_6\text{O}_4]^+$, respectively. The peak observed at m/z 532.10 was attributed to molecular ion, $[\text{C}_{26}\text{H}_{20}\text{CrN}_6\text{O}_4]^+$. Complex **3** exhibits peaks at m/z 269.10, 347.93, 390.99 and 409.96 attributed to $[\text{C}_{15}\text{H}_{15}\text{N}_3\text{O}_2 + 2\text{H}^+]^+$, $[\text{C}_{10}\text{H}_{11}\text{Cl}_3\text{CrN}_2\text{O}_2]^+$, $[\text{C}_{15}\text{H}_{15}\text{Cl}_2\text{CrN}_3\text{O}_2]^+$, and $[\text{C}_{15}\text{H}_{15}\text{Cl}_3\text{CrN}_3\text{O}_2 + \text{H}^+]^+$, respectively. The peak at m/z 409.96 was attributed for pseudo-molecular ion, $[\text{C}_{15}\text{H}_{15}\text{Cl}_3\text{CrN}_3\text{O}_2 + \text{H}^+]^+$. However, complex **4** exhibits peaks at $m/z = 256.10$ and 560.13 attributed to $[\text{C}_{14}\text{H}_{12}\text{N}_6\text{O}_4 + 2\text{H}^+]^+$ and $[\text{C}_{28}\text{H}_{24}\text{CrN}_6\text{O}_4]^+$, respectively. The peak at m/z 560.13 was due to molecular ion $[\text{C}_{28}\text{H}_{24}\text{CrN}_6\text{O}_4]^+$, indicating the ionic nature of complex. Since naturally occurring chromium is composed of four stable isotopes (^{50}Cr , ^{52}Cr , ^{53}Cr , and ^{54}Cr with ^{52}Cr being the most abundant (83.789% natural abundance)), ESI-MS spectrum of **4** (figure S7) clearly shows four peaks at m/z 558.13, 560.12, 561.13 and 562.13 assigned for $[\text{M}^+]^+$ ion peaks of the four isotopes.

FT-IR spectra of ligands display characteristic one/two peaks between $1610\text{-}1618\ \text{cm}^{-1}$ assigned to a combination of $\nu(\text{C}=\text{N}) + \nu(\text{HC}=\text{N})$. This peak was shifted in complexes **1-4** and

appeared in the range 1604-1570 cm^{-1} , clearly indicating coordination to metal through imine-N [51]. Ligands L_1 and L_2 exhibit a weak peak at 3350 cm^{-1} and 3352 cm^{-1} , respectively, assigned for $\nu(\text{-OH})$, which vanished in complexes **1**, **2**, **3** and **4** and new peaks appeared at 428, 464, 430 and 426 cm^{-1} , respectively, attributed for new $\nu(\text{M-O})$ bond indicating the bonding of metal to the oxygen. A signal exhibited in **1** and **3** at 771 cm^{-1} and 778 cm^{-1} , respectively, was attributed to wagging and rocking mode of coordinated water [52]. FT-IR spectrum of **4** is given in figure S3.

Electronic spectra of complexes (10^{-3} M) were measured in DMSO. Complexes **1-4** are paramagnetic with magnetic susceptibility in between 3.65-3.80 BM. The electronic spectra of L_1 and L_2 exhibit three bands at 220 nm, 260 nm and 300 nm. The first band was assigned to the $\pi\text{-}\pi^*$ transition of the C=C chromophore, however, the other two bands are assigned to the $n\text{-}\pi^*$ transition associated with C=N and C=O groups, respectively. The first band assigned to C=C chromophore and auxochrome of benzene ring was red-shifted in the complexes and appeared at 260 nm in the complexes. The other two bands assigned to $n\text{-}\pi^*$ transition of $(\text{C=N})_{\text{imine}}$ and C=O groups are also red-shifted and appeared with decreased intensity at 280 nm and 340 nm in the complexes, indicating an interaction of the ligand with metal ion due to the transfer of a non-bonding electron pair from donor to metal. In the electronic spectra of the complexes, two low-intensity broad bands appeared at 420 and 460 nm, attributed to the d-d transitions ${}^4\text{A}_{2g} \rightarrow {}^4\text{T}_{2g}$ (ν_1) and ${}^4\text{A}_{2g} \rightarrow {}^4\text{T}_{1g}$ (ν_2) of the Cr(III) ion. These bands are of low molar absorptivity (ϵ) being 'Laporte forbidden' transitions. However, in chromium complexes, two transitions bands are observed in the region as expected, but the third transition, ${}^4\text{A}_{2g} (\text{F}) \rightarrow {}^4\text{T}_{1g} (\text{P})$, could not be identified; it may lie in the ligand field. The electronic spectral transition suggests an octahedral environment around Cr(III) ion [53]. Electronic spectrum of **4** is shown in figure S8.

Since all complexes were paramagnetic, NMR spectra of the complexes were complicated. The theory of the unpaired electron-nucleus interaction and its consequences for NMR spectroscopy has been developed over the past decades and has been summarized to some extent. In diamagnetic molecules, the orbital shift (d_{orb}) provides the principal contribution to the observed chemical shifts. In paramagnetic samples, the hyperfine shift (d_{hf}) adds to the orbital shift, leading to the observed chemical shift:

$$d_{obs} = d_{orb} + d_{hf}$$

In view of common evidence and inevitable paramagnetic interference, we have explained ¹H-NMR spectra of **4** (figure S9). A comparison of signals of the ligand with complexes reveals that there are four signals between 2.452 ppm and 11.489 ppm. The two very weak and broad signals between 6.80 ppm to 7.80 ppm can be attributed to phenolic protons. However, a signal observed at 8.70 ppm was assigned to pyridyl protons. Signals expected for methyl proton not observed in the normal scale may be due to paramagnetic interference. A signal at 11.489 ppm was assigned to CONH proton. Signal observed at 13.188 ppm for one phenolic-OH proton in L₂ vanished in **4**, indicating removal of O-H proton and formation of M-O bond [54, 55]. 2D-HSQC of **4** was not appropriate.

3.3. Stability constants of the complexes

The stoichiometries of reactions and complexing behavior of Schiff base ligands with chromium Job's method of continuous variation [56] was used in the investigation of composition and stability constant of complexes during the reaction. The stability constants (K) for **1**, **2**, **3** and **4** were 1.919×10^3 , 2.473×10^5 , 1.266×10^3 and 2.011×10^5 M⁻¹, respectively. From the close observation of the data it was clearly observed that stability constants of **2** and **4** are quite high, which may be ascribed to their 1:2 metal ratio. Job's plot of **4** is shown in figure 2 and Job's plots of **1-3** are shown in figures S10-S12.

The Gibb's free energy of formation of complexes is also calculated from the relationship:

$$\Delta G = -RT \ln K$$

where R is the gas constant (8.314 J/mole K), T is absolute temperature (273.16 + 25 = 298.16 K) and K is stability constant. The Gibbs free energies of **2** and **4** are also highly negative, which indicate more feasibility of formation of these complexes in solution. Thermodynamic and coordinating parameters of all complexes are presented in table S2.

3.4. DFT calculations

3.4.1. Molecular geometry, bond length and bond angles. In order to achieve better insight into the molecular structure of ligands L₁ and L₂ and complexes **1-4**, computational analysis has

been performed, which is designed for the realization of large-scale DFT calculations. It was clearly observed from the fully-optimized structure of ligands that in both ligands (figure 3) benzene ring is not in the plane of pyridyl ring, but actually situated at $\sim 45^\circ$ angles. The molecular structure of complexes shows almost octahedral geometry around Cr(III) ion as it was revealed from the bond distances and bond angles (table 1). Some bond length becomes slightly longer than ligands. Since ligand was coordinated through azomethine-N and formation of an M-N bond takes place, elongation in azomethine C=N was observed due to a partial shift in electron density towards M-N bond. Similarly, coordination was also observed from the deprotonated oxygen of hydroxybenzylidene moiety and the carbonyl oxygen of isonicotinyl hydrazide. It was interestingly observed that pyridyl and benzene ring which were not in the same plane in ligands were rotated and moved closer to each other in order to facilitate coordination with metal. However, small angular distortions were observed in N-Cr-O, Cl-Cr-Cl, O-Cr-O, O-Cr-Cl and N-Cr-N bond angles.

3.4.2. Quantum chemical parameters. The quantum chemical parameters; highest occupied molecular orbital energy (E_{HOMO}), lowest unoccupied molecular orbital energy (E_{LUMO}), the difference between HOMO and LUMO energy levels (ΔE), Mulliken electronegativity (χ), dipole moment chemical potential (μ), global hardness (η), global softness (S), global electrophilicity (ω), absolute softness (σ) and electronic charge (ΔN_{max}) have been estimated and listed in table 2.

On the basis of the above data, we can conclude that:

1. The value of energy gap (ΔE) is higher in L_1 than L_2 , which indicates the hard nature as well as low reactivity of L_1 .
2. Complexes **2** and **4** exhibit lower energy gap than other complexes, which indicates their soft nature, high reactivity and high flexibility in the transfer of electrons from a donor (ligand) to acceptors (metal ions).
3. The E_{LUMO} value was low in L_2 which is an indicator of high acceptability for electrons. The E_{LUMO} values were almost the same in complexes.
4. The high value of E_{HOMO} was observed in L_2 which may be due to its powerful donation behavior. Global hardness (η) and absolute softness (σ) parameters are the

indicators of molecular stability and reactivity. The negative data of both E_{LUMO} and E_{HOMO} were attributed to the stability of the complexes.

3.4.3. Mulliken atomic charge analysis. The Mulliken population analyses of ligands and complexes **1-4** were done by using method B3LYP/6-311++G(d, p) with LANL2DZ basis set in the gas phase. The net atomic charges of ligands and their complexes were obtained by means of Mulliken population analysis. Mulliken charge is directly related to the vibrational properties of the molecule. Distribution of positive and negative charges are the major cause to increase or decrease bond length. The result shows that L_1 has more positive charges on carbon atom C13 (+0.469029) due to the highly electronegative imine N11 (-488796) and O25 (-415137) attached to this carbon atom. One positively charged carbon C15 (+0.202289) and one hydrogen H29 (+0.374521) are connected to more electronegative phenolic oxygen O26 (-0.625646) of the benzene ring. However, in L_2 more positive charges appear on carbon atom C13 (+0.411532) because this atom is connected to more electronegative nitrogen N11 (-0.463831) and oxygen O25 (-0.596106). Another positively charged carbon atom C15 (+0.169524) and hydrogen atom H27 (+0.320235) is connected with the more electronegative phenolic O26 (-0.596106) of the benzene ring. This is due to highly shielded atoms such as oxygen and nitrogen attached to less electronegative or positively charged atoms such as carbon and hydrogen, acquiring a highly negative charge. However, in **1-4**, chromium(III) ion carries higher positive charge, +1.095398, +1.245587, +1.712005 and +1.456922, respectively. Therefore, in **1** and **3**, three electronegative atoms, an oxygen atom of CONH moiety, another oxygen atom of dehydrogenated hydroxyl moiety and an imine nitrogen of ligands are points of coordination with the electropositive metal centered. Of the remaining three coordinating sites, two coordinating points were occupied by chloride ion and one coordinating point was occupied by the oxygen atom of a neutral water molecule. However, in **2** and **4**, six electronegative atoms which are two phenolic oxygen atoms, two imine nitrogen atoms and two oxygen of CONH moiety of ligands are coordinating points with an electropositive metal center. Mulliken charge values of electropositive carbon and electronegative oxygen/nitrogen atoms are also higher than ligand, probably due to an occurrence of back-bonding of π -electrons during complex formation. This result is consistent with the molecular electrostatic potential (MEP) [57-59]. The illustration of atomic charges for L_2 and **4** are shown as bar diagrams in figure S13.

3.4.4. Molecular electrostatic potential analysis (MEP) and contour maps. The MEP is related to electron density and provides information about electron rich and electron deficient sites in the molecules, which is a very useful description to understand metal-ligand interactions as well as hydrogen bonding. The negative regions in MEP are related to the electronegative site, while the positive regions are related to the electropositive site. The MEP of the ligand molecule shows several regions of positive and negative potential. The negative regions are mainly over the oxygen and nitrogen atoms (deep red/yellow) on -CONH groups of INH moiety and nitrogen atoms of imine groups of ligand. Most positive regions (blue/green) are observed around the hydrogen atoms of C-H groups as well as carbon atoms of imine groups. The color codes of this map are in the ranges -0.0723 a.u. (deep red) to +0.0723 a.u. (deep blue) in L₁ and -0.0755 a.u. (deep red) to +0.0755 a.u. (deep blue) in L₂. In **1** and **3**, MEP is between -0.0012 a.u. (deep red) to +0.0012 a.u. (deep blue) and -0.0010 a.u. to +0.0010 a.u., respectively. However, in **2** and **4** MEP is between -0.0752 a.u. to +0.0752 a.u. and -0.0775 a.u. to +0.0775 a.u., respectively. The potential increases in the order: red < orange < yellow < green < blue. The different colors represent the different values of the electrostatic potential at the different atomic surface. Molecular electrostatic potentials of L₂ and **4** are shown in figure 4.

On the basis of the elemental analysis, molar conductance measurements, magnetic susceptibility, ESI-MS, electronic, FT-IR, ¹H-NMR, ²D-NMR spectra and DFT studies, the most plausible ChemDraw structure and DFT optimized structure of complex **4** is shown in figure 5 and of complexes **1-3** in figures S14-S16.

3.5. Biological activity

3.5.1. *In vitro* antioxidant activity of ligands (free radical scavenging activity). The antioxidant activity of the ligands was examined by measuring the scavenging effect of DPPH radicals. The results of the free radical scavenging activity of the compounds at different micromolar concentrations are shown in table 3. Ascorbic acid was used as a control to estimate the effectiveness of the tested compounds under the same conditions. It was observed that the free radical scavenging activity of these compounds was concentration-dependent. The examined compounds have exhibited significant scavenging activity but lower than ascorbic acid. It has

been observed that L₂ exhibited higher antioxidant activity of about 5-8% at every concentration than L₁.

3.5.2. *In vitro* antidiabetic activity. *In vitro* antidiabetic activity results are displayed in table 4.

A close observation of data reveals that:

1. Complexes exhibit better inhibition efficiency than Schiff base ligands.
2. Complexes **3** and **4** exhibit high inhibition efficiency. However, inhibition efficiency of **4** was almost the same as acarbose, used as a standard for comparison. It may be due to a synergistic combination of L₂ to chromium(III) ion, in particular steric environment results in better absorption at the surface of the enzyme leading to better inhibition.
3. However, complexes **1** and **2** exhibited less inhibiting activity than expected. These complexes show inhibition efficiency just above the ligand, probably due to the fact that congregation of some function present in ligand in combination with chromium(III) in a particular steric environment may not work in a synergistic way for the improvement of antidiabetic activity.

3.5.3. *In vivo* antidiabetic activity. To assess the *in vivo* antidiabetic activity of chromium complexes, the animal study was carried out on *Albino wistar* rats. The glucose level and body weight were monitored before and after the treatment with the complex. The standard drug glibenclamide was used for the comparison. Antioxidant activity and histology of pancreas were studied on the twenty-first day in order to observe the effect of the drug on the animal.

3.5.3.1. *Body mass of rats.* The body weight of each group of rats before and after treatment with the complex is shown in figure S17. The body weight of diabetic rats (Group 2) reduced with time as compared to the initial weight. In the case of non-diabetic control rats (Group 1), weight gain was observed. However, the body weight of complex-treated groups (Group 4 and Group 5) and standard drug glibenclamide-treated group (Group 3) were significantly lowered initially in the first week because of lower food and water consumption (first three days after drug administration) and thereafter, considerably increases throughout the experiment.

3.5.3.2. *Blood glucose level.* The blood glucose levels before and after treatment are shown in table 5 and figure S18. There is a significant gradual decrease in the glucose level observed after the treatment with the complex. The percentage of decrease in glucose level was slightly higher in Group 5, indicating the effect of a high dose of **4** to mice. However, in standard mice group treated with antidiabetic drug glibenclamide, a sudden decrease in glucose level was observed in the first seven days and thereafter decrease in blood glucose level was steady. The glucose level of diabetic rats (Group 2) increases throughout the experiment.

3.5.3.3. *Histological analysis.* Histology of pancreas was analyzed on the basis of an effect on the islet of Langerhans (figure 6). In animals treated with the standard drug, normal intercalated ducts were clearly observed in histological slides 1 and 2, interlobular duct, acini, blood vessels and pancreatic islets were distinguished from surrounding exocrine tissue on the basis of continuous connective tissue capsule and extensive vascularity. Similarly, in the complex-treated group, histology is almost the same. In the diabetic group at some location, alteration in the structural morphology of islets was observed. Interestingly, it can be easily observed that in Group 5 animals, which were treated with higher dose of the complex (200 mg/kg), histology of pancreas is exactly similar to normal group animal.

3.5.4. *In vivo* antioxidant activity of complex. Complex **4** was also tested for antioxidant activity for lipid peroxides (LPO), superoxide dismutase (SOD), glutathione (GSH) and catalase (CAT) on the twenty-first day. It was observed that complex-treated groups (Group 4 and 5) have higher levels of antioxidative parameters (catalase, superoxide dismutase and glutathione) and decreased levels of lipid peroxidation, indicating its efficacy to reduce the LDL-c oxidation. In the complex-treated groups, a significant increase in the liver CAT, SOD and reduced GSH levels were observed as compared to the STZ control animals, which suggests good antioxidant activity of this complex. *In vivo* antioxidant activity is shown in table 6.

3.5.5. Antibacterial screening of ligands and complex. The results of *in vitro* antibacterial activity of the Schiff base ligands and their complexes **1-4** are presented in table 7. Amoxicillin was used as positive standards and DMSO was used as negative control for this antibacterial activity. Metal complexes have been more effective than the free ligands. Complex **4** displayed

the highest bactericidal activity against *E. coli*. However, other complexes exhibit lower antibacterial activity [60]. The activity order of the synthesized compounds was as follows: **4** > **3** > **2** > **1** > **L₂** > **L₁**. It is postulated that improved activity arises from the delocalization of positive charge between the organic moiety and the metal, which favors the drug entering into normal cellular processes of the bacteria. Probably the enhanced lipophilicity of the complexes leads to breakdown of the permeability barrier of the cell and thus retards the normal cell process in bacteria. The minimum inhibitory concentration (MIC) of the complexes is also displayed in the table 7 since the MIC is the concentration of the highest dilution tube, in which bacterial growth was absent. It was observed that **1-4** has exhibited MIC in between 31-37 µg/mL.

4. Conclusion

Two Schiff bases and their four chromium(III) complexes were synthesized and characterized by spectroscopic techniques. Higher stability constant values of **2** and **4** suggested high stability of 1:2 metal chelate complexes. Gibbs free energy (ΔG) of these complexes is also high, which suggests high feasibility of their formation reaction. DFT was used to achieve better insight into molecular structure. These compounds were initially studied for their *in vitro* antidiabetic and antioxidant activity. Complexes **3** and **4** have exhibited a very promising *in vitro* antidiabetic activity. Complex **4** shows *in vitro* antidiabetic activity almost the same as acarbose and was selected for *in vivo* antidiabetic and antioxidant activity in *Albino wistar* rats. A significant gradual decrease in the blood glucose level was observed in complex-treated groups. It was also observed that complex-treated groups have higher levels of antioxidative parameters (catalase, superoxide dismutase and glutathione) and decreased levels of lipid peroxidation, indicating its efficacy to reduce the LDL-c oxidation. In the complex-treated groups, a significant increase in the liver CAT, SOD and reduced GSH levels were observed as compared to the STZ control animals, which suggests the good antioxidant activity of this complex. Interestingly, it was also obvious from the histological slides that the group treated with a high dose of the complex has the same histology as normal. It means higher doses of complex helps in maintaining the health of the pancreas. In view of such promising results, we can say that this therapeutic approach may be used as an important strategy in the management of blood glucose. Thus, the study of these compounds is quite interesting not only in terms of their reactivity but also due to their varied range of activity.

Acknowledgements

The authors are grateful to Principal, Government Science College, Jabalpur and Head, Chemistry Department, for providing laboratory facilities. We sincerely thank SAIF, CDRI, Lucknow, for recording ESI-MS, ¹H-NMR spectra. We are also thankful to Daksh laboratory, Jabalpur and PBRI, Bhopal for their valuable help rendered in *in-vitro* and *in-vivo* activity. One of us (Sangeeta Jhariya) is also grateful to the UGC-New Delhi for financial support through RGNF (Award letter no. F1-17.1/2015-16/RGNF-2015-17-SC-MAD-19472/ (SA-III/Website)).

References

- [1] P. Zimmet, K.G. Alberti, J. Shaw. *Nature*, **414**, 782 (2001).
- [2] WHO report of world diabetes day, “*Eastern Mediterranean Region*” WHO (2013).
- [3] D.T. Jakusch, D. Hollender, E.A. Enyedy, C.S. Gonzalez, M.M. Bayon, A.S. Medel, J.C. Pessoa, I. Tomaz, T. Kiss. *Dalton Trans.*, **13**, 2428 (2008).
- [4] J.S. Shaw, R.L. Wilmot, E.S. Kilpatrick. *Diabet. Med.*, **24**, 1160 (2007).
- [5] W.G. Herrington, J.B. Levy. *Int. Urol. Nephrol.*, **40**, 411 (2008).
- [6] M. Peng, X. Yang. *J. Inorg. Biochem.*, **146**, 97 (2015).
- [7] K. Hariprasath, B. Deepthi, I. Sudheer Babu, P. Venkatesh, S. Sharfudeen, V. Soumya. *J. Chem. Pharm. Res.*, **2**, 496 (2010).
- [8] W. Feng, T. Zhao, G. Mao, W. Wang, Y. Feng, F. Li, D. Zheng, H. Wu, D. Jin, L. Yang, X. Wu. *Plos One*, **10**(5), (2015).
- [9] D. Ghosh, B. Bhattacharya, B. Mukherjee, B. Manna, M. Sinha, J. Chowdhury, S. Chowdhury. *J. Nutr. Biochem.*, **13**, 690 (2002).
- [10] G.M. Reaven. *Diabetes*, **37**, 1595 (1998).
- [11] Z. Krejpcio. *Polish J. Environ. Stud.*, **10**, 399 (2001).
- [12] J.B. Vincent, *The Nutritional Biochemistry of Chromium(III)*, Elsevier, 139-151 (2007).
- [13] C. Peloquin. *Medical Clinics of North America*, **77**, 1253 (1993).
- [14] J. Sandy, S. Holton, E. Fullam, E. Sim, M. Noble. *Protein Sci.*, **14**, 775 (2004).
- [15] S.N. Shukla, P. Gaur, S. Mathews, S. Khan, A. Srivastava. *J. Coord. Chem.*, **61**, 3913 (2008).
- [16] A.H.E. Masry, H.H. Fahmy, S.H.A. Abdelwahed. *Molecules*, **5**, 1429 (2000).

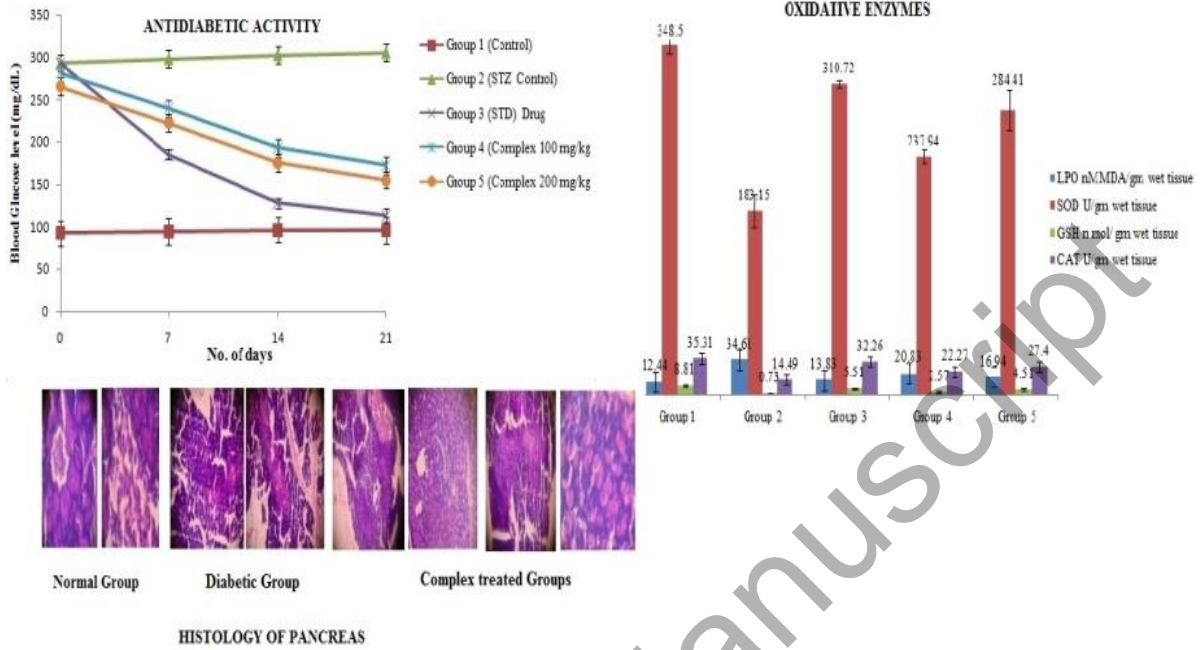
- [17] M.A. Baseer, V.D. Jadhav, R.M. Phule, Y.V. Archana, Y.B. Vibhute. *Orient. J. Chem.*, **16**, 553 (2000).
- [18] S.N. Pandeya, D. Sriram, G. Nath, E. De Clercq. *II Farmaco*, **54**, 624 (1999).
- [19] E.M. Hodnett, W.J. Dunn. *J. Med. Chem.*, **13**, 768 (1970).
- [20] S.B. Desai, P.B. Desai, K.R. Desai. *Heterocycl. Commun.*, **7**, 83 (2001).
- [21] P. Pathak, V.S. Jolly, K.P. Sharma. *Orient. J. Chem.*, **16**, 161 (2000).
- [22] J. Vanco, J. Marek, Z. Travnicek, E. Racanska, J. Muselik, O. Svajlenova. *J. Inorg. Biochem.*, **102**, 595 (2008).
- [23] S. Samadhiya, A. Halve. *Orient. J. Chem.*, **17**, 119 (2001).
- [24] N.P. Priya, S. Arunachalam, A. Manimaran, D. Muthupriya, C. Jayabalakrishnan. *Spectrochim. Acta. Part A*, **72**, 670 (2009).
- [25] H.J. Kim, W. Kim, A.J. Lough, B.M. Kim, J.A. Chin. *J. Am. Chem. Soc.*, **127**, 1676 (2005).
- [26] J.P. May, R. Ting, L. Lermer, J.M. Thomas, Y. Roupioz, D.M. Perrin. *J. Am. Chem. Soc.*, **126**, 4145 (2004).
- [27] G.H. Jeffery, J. Bassett, J. Mendham, R.C. Denney, *Vogel's Textbook of Quantitative Chemical Analysis, fifth Edition* 454 (1989).
- [28] K.K. Deshmukh, A.M. Hundekar, D.N. Sen. *J. Ind. Chem. Soc.*, **57**, 1147 (1980).
- [29] P. Job. *Ann. Chim.*, **9**, 113 (1928).
- [30] Q. Yao, C. Li, H. Huang, H. Chen, B. Liu. *J. Mol. Struct.*, **1143**, 371 (2017).
- [31] Gaussian 09, Revision C.01, M.J. Frisch, G.W. Trucks, H.B. Schlegel, G.E. Scuseria, M.A. Robb, J.R. Cheeseman, G. Scalmani, V. Barone, B. Mennucci, G.A. Petersson, H. Nakatsuji, M. Caricato, X. Li, H.P. Hratchian, A.F. Izmaylov, J. Bloino, G. Zheng, J.L. Sonnenberg, M. Hada, M. Ehara, K. Toyota, R. Fukuda, J. Hasegawa, M. Ishida, T. Nakajima, Y. Honda, O. Kitao, H. Nakai, T. Vreven, J.A. Montgomery, Jr., J.E. Peralta, F. Ogliaro, M. Bearpark, J.J. Heyd, E. Brothers, K.N. Kudin, V.N. Staroverov, T. Keith, R. Kobayashi, J. Normand, K. Raghavachari, A. Rendell, J.C. Burant, S.S. Iyengar, J. Tomasi, M. Cossi, N. Rega, J.M. Millam, M. Klene, J.E. Knox, J.B. Cross, V. Bakken, C. Adamo, J. Jaramillo, R. Gomperts, R.E. Stratmann, O. Yazyev, A.J. Austin, R. Cammi, C. Pomelli, J.W. Ochterski, R.L. Martin, K. Morokuma, V.G. Zakrzewski, G.A. Voth, P.

- Salvador, J.J. Dannenberg, S. Dapprich, A.D. Daniels, O. Farkas, J.B. Foresman, J.V. Ortiz, J. Cioslowski, D.J. Fox, *Gaussian, Inc.*, Wallingford CT (2010).
- [32] W.M.I. Hassan, E.M. Zayed A.K. Elkholy, H. Moustafa, G.G. Mohamed. *Spectrochim. Acta, Part A*, **103**, 378 (2013).
- [33] F.A.I. Al-Khodir, M.S. Refat. *J. Mol. Struct.*, **1094**, 22 (2015).
- [34] Q.M. Hasi, Y. Fan, X.Q. Yao, D.C. Hu, J.C. Liu. *Polyhedron*, **109**, 75 (2016).
- [35] N. Uddin. *J. Trop. Biomed.*, **4**, 473 (2014).
- [36] J. Kamboj, S. Sharma, S. Kumar. *J. Health Sci.*, **57**, 225 (2011).
- [37] R. Yanardag, T.B. Demirci, B. Ulkuseven, S. Bolkent, S. Tunalı, S. Bolkent. *Eur. J. Med. Chem.*, **44**, 818 (2009).
- [38] E.U. Etuk. *Agric. Biol. J. N. Am.*, **1**, 130 (2010).
- [39] M.A. Mahmoud, S.A. Zaitone, A.M. Ammar, S.A. Sallam. *J. Mol. Struct.*, **1108**, 60 (2015).
- [40] H. Ohkawa, N. Ohishi, K. Yagi. *Anal. Biochem.*, **95**, 35 (1979).
- [41] V.D. Sapakal, T.S. Shikalgar, R.V. Ghadge, R.S. Adnaik, N.S. Naikwade, C.S. Magdum. *A Review, J. Herbal Med. Toxicol.*, **2**, 1 (2008).
- [42] L. Goth. *Clin. Chim. Acta*, **196**, 143 (1991).
- [43] F. Paoletti, D. Aldinucci, A. Mocali, A. Caparrini. *Anal. Biochem.*, **153**, 536 (1986).
- [44] M.S. Refat, S.M.E. Megharbel, M.A. Hussien, R.Z. Hamza, M.A. Al-Omar, A.M. Naglah, W.M. Afifi, M.I. Kobeasy. *Spectrochim. Acta, Part A*, **173**, 122 (2016).
- [45] C.A. Ekennia, A.A. Osowole, O.L. Olasunkanmi, C.D. Onwudiwe, O.O. Olubiyi, E.E. Ebenso. *J. Mol. Struct.*, **1150**, 279 (2017).
- [46] M.K. Kumar, S. Prabhakar, M.R. Kumar, T.J. Reddy, S. Premsingh, S. Rajagopal, M. Vairamani. *Rapid Commun. Mass Spectrom.*, **18**, 1103 (2004).
- [47] N.S. Biradar, V.L. Roddabasanagoudar, T.M. Aminabhavi. *Polyhedron*, **3**, 575 (1984).
- [48] B.R. James, R.H. Morris. *Can. J. Chem.*, **58**, 399 (1980).
- [49] W.J. Geary. *Coord. Chem. Rev.*, **7**, 81 (1971).
- [50] V. Katta, S.K. Choudhury, B.T. Chait. *J. Am. Chem. Soc.*, **112**, 5348 (1990).
- [51] K.K. Deshmukh, A.M. Hundekar, D.N. Sen. *J. Ind. Chem. Soc.*, **57**, 1147 (1980).
- [52] M.S. Sujamol, C.J. Athira, Y. Sindhu, K. Mohanan. *Spectrochim. Acta, Part A*, **75**, 106 (2010).

- [53] A.A.A. Emara, A.A. Saleh, O.M.I. Adly. *Spectrochim. Acta, Part A*, **68**, 592 (2007).
- [54] P.K.L. Chan, B.R. James, D.C. Frost, P.K.H. Chan, H.L. Hu, K.A. Stov. *Can. J. Chem.*, **279**, 395 (1985).
- [55] F.D. Rochan, D.C. Kang, L. Giral. *Can. J. Chem.*, **64**, 1897 (1986).
- [56] O. Altun, M. Suozer. *J. Mol. Struct.*, **1149**, 307 (2017).
- [57] V. Krishnakumar, K. Murugeswari, N. Prabavathi, R. Mathammal, *Spectrochim. Acta, Part A*, **91**, 1 (2012).
- [58] S. Tabti, A. Djedouani, D. Aggoun, I. Warad, S. Rahmouni, S. Romdhane, H. Fouzi. *J. Mol. Struct.*, **1155**, 11 (2017).
- [59] M. Khajehzadeh, N. Sadeghi. *J. Mol. Liq.*, **249**, 281 (2017).
- [60] S.N. Shukla, P. Gaur, N. Rai. *Appl. Nanosci.*, **5**, 583 (2015).

Accepted Manuscript

Graphical abstract



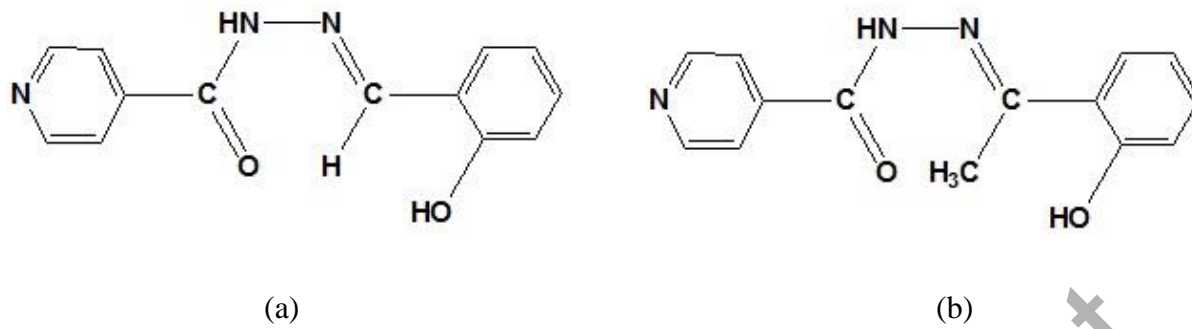


Figure 1. Structure of (a) *(E)*-*N'*-(2-hydroxybenzylidene) isonicotinohydrazide (**L**₁) and (b) *(E)*-*N*-(1-(2-hydroxyphenyl) ethylidene)isonicotinohydrazide (**L**₂).

Accepted Manuscript

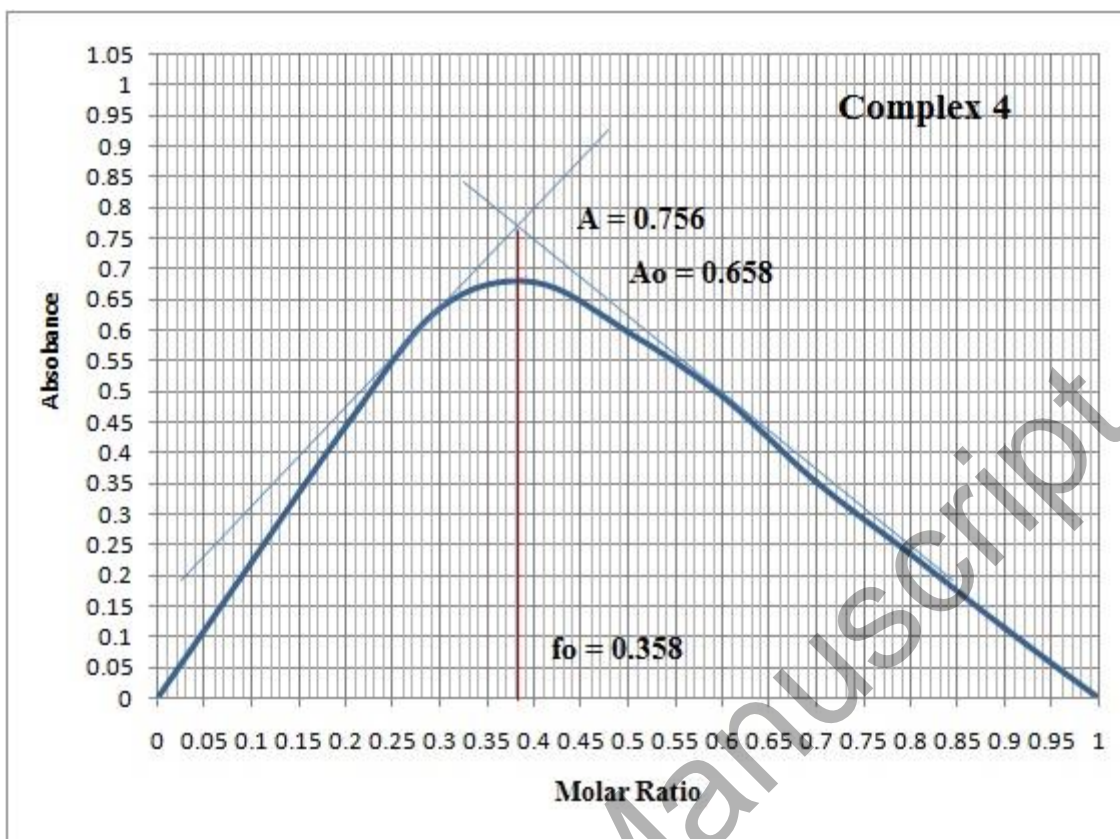


Figure 2. Job's plot of complex 4.

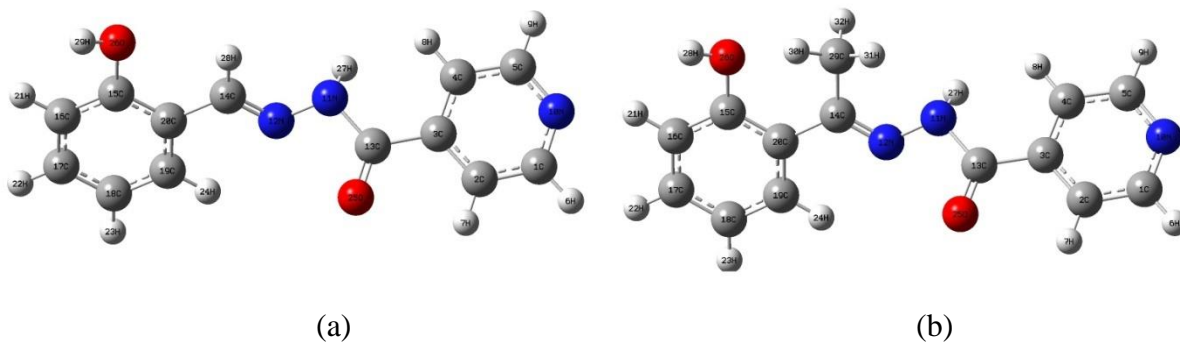


Figure 3. DFT optimized structure of (a) *(E)*-*N'*-(2-hydroxybenzylidene)isonicotinyl hydrazide (**L**₁) and (b) *(E)*-*N*-(1-(2-hydroxyphenyl) ethylidene)isonicotinyl hydrazide (**L**₂).

Accepted Manuscript

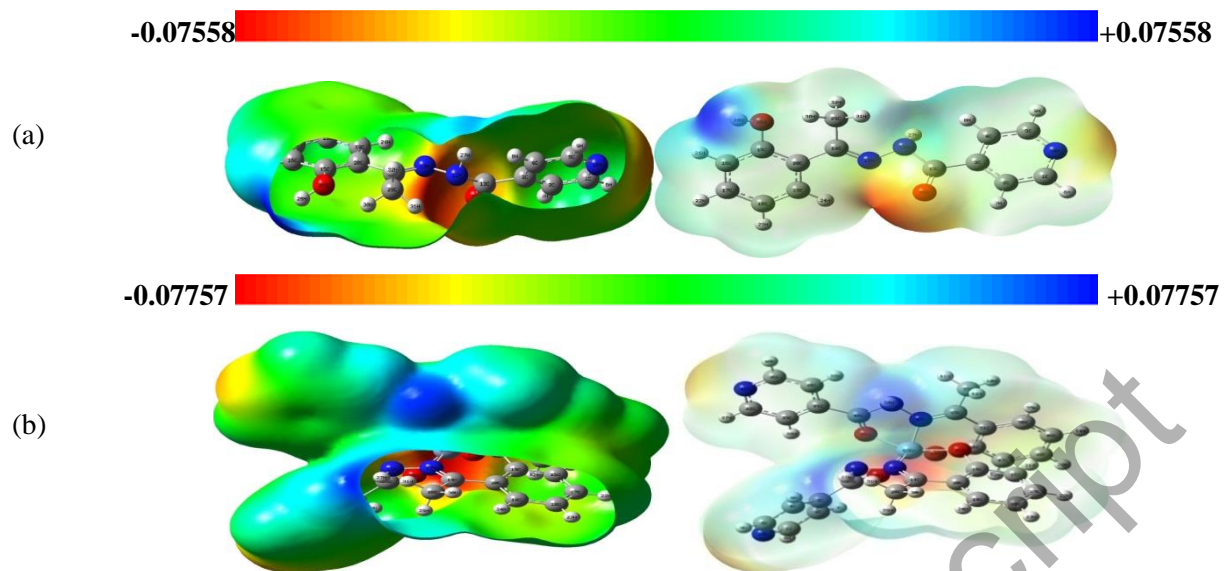
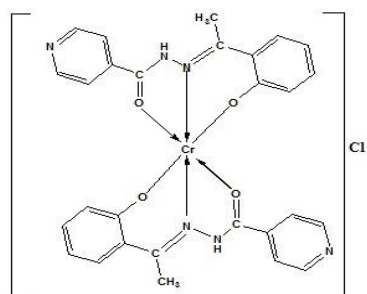
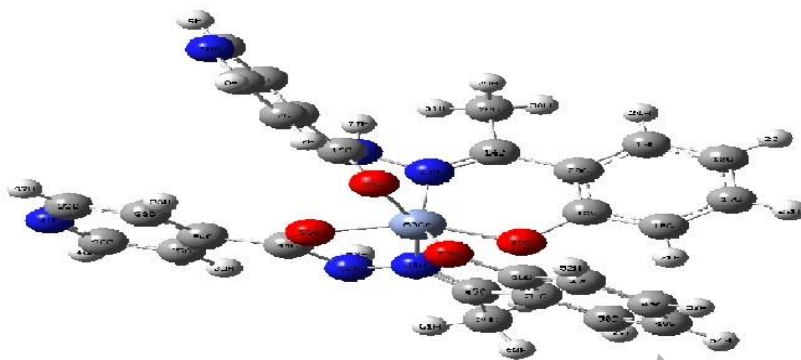


Figure 4. Molecular Electrostatic Potential (MEP) of (a) L₂ and (b) complex 4.



(a)



(b)

Figure 5. (a) Chemical structure and (b) DFT optimized structure of complex 4.

Accepted Manuscript

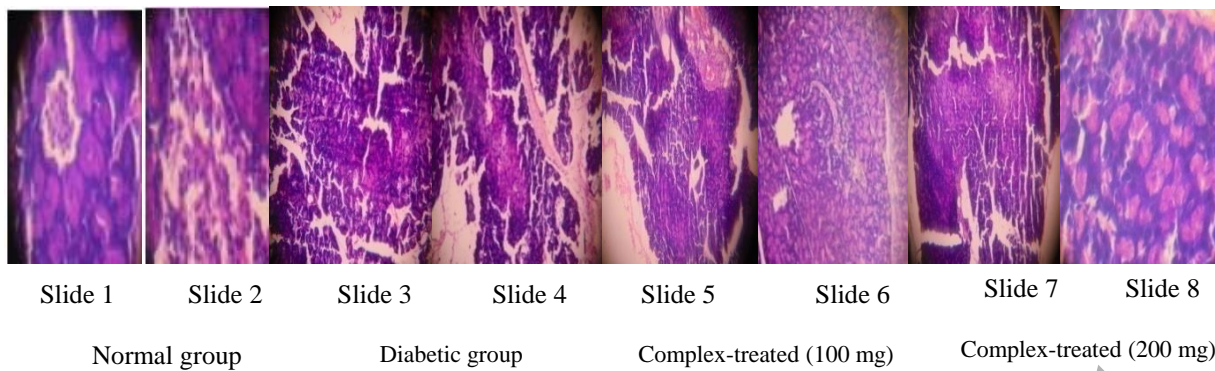


Figure 6. Histology of pancreas.

Accepted Manuscript

Table 1. Selected geometrical parameters of ligands and complexes.

Bond connectivity	Bond length (in angstrom)					
	L ₁	L ₂	1	2	3	4
C=N	1.293	1.293	1.321	1.288	1.284	1.288
C=O	1.258	1.258	1.308	1.260	1.312	1.260
C-O	1.430	1.430	1.430	1.448	1.441	1.445
O-H	0.960	0.960	-	---	----	----
M-O	-	----	1.783	1.838	1.788	1.767
M-N	----	----	1.815	1.820	1.824	1.810
M-Cl	----	----	2.120	----	2.120	----
M-O(H ₂ O)	----	----	1.790	----	1.790	----
M-O coordination	----	----		1.819		1.819
Bond connectivity	Bond angle					
N-N=C	119.999	119.999	122.977	122.977	122.910	122.909
N-C=O	120.000	120.00	115.848	115.848	114.864	114.870
H-C=C	120.308	120.308	119.925	119.694	119.931	120.310
C=N-C _(pyridyl ring)	121.464	121.464	121.465	121.456	121.464	121.464
H-O-C _(benzene ring)	109.471	109.471	----	----	----	----
C-C=C	119.383	119.383	119.389	118.832	118.833	118.829
C-C=C	120.000	120.00	120.040	120.040	119.967	120.154
N-Cr-O			82.988	77.953	80.675	77.920
Cl-Cr-Cl			88.890	---	93.415	----
O-Cr-O			98.332	71.631	90.863	77.355
O-Cr-Cl			91.089	----	87.136	----
Cr-N-C			121.078	----	112.165	----
N-Cr-N			----	107.545	----	107.801
Bond connectivity	Dihedral angle					
C=N-N-C	149.999	149.999	160.351	158.598	140.364	158.593
H-N-C=O	-149.999	-149.999	-125.254	-125.536	-125.377	125.534
C-O-Cr-O	----	----	---	151.141		151.141
H-C-N-C	179.987	179.987	179.987	179.998	179.999	179.988
H-C-Cr-Cl	----	----	63.836	----	63.836	----
H-O-Cr-O	----	----	109.685	----	109.685	----

Table 2. Quantum chemical parameters of ligands and their complexes.

Parameter	L ₁	L ₂	1		2	3		4
			α - MOs	β - MOs		α - MOs	β - MOs	
Total energy (a.u.) E(TD-HF/TD-KS)	-816.267	-855.668	-2857.284	-2857.284	-2676.702	-2896.882	-2896.882	-2754.819
Dipole moment	4.572	5.442	10.940	10.940	6.937	8.235	8.235	8.528
E _{HOMO} (eV)	-6.244	-5.051	-5.252	-5.628	-4.211	-6.273	-5.046	-4.045
E _{LUMO} (eV)	-1.891	-2.525	-3.550	-3.603	-2.868	-3.704	-2.997	-2.671
ΔE (eV)	4.353	2.526	1.702	2.025	1.343	2.569	2.049	1.374
χ (eV)	4.067	3.788	4.401	4.615	3.539	4.988	4.021	3.358
η (eV)	2.176	1.263	0.851	1.039	0.671	1.284	1.024	0.687
σ (eV)	0.459	0.791	1.175	0.962	1.490	0.778	0.976	1.455
Pi (eV)	-4.067	-3.788	-4.401	-4.615	-3.539	-4.988	-4.021	-3.358
S (eV)	0.229	0.395	0.587	0.481	0.745	0.389	0.488	0.727
ω (eV)	3.800	5.680	11.380	10.249	9.332	9.688	7.894	8.206
ΔN_{\max} (eV)	1.869	2.999	5.171	4.441	5.274	3.884	3.926	4.887

Table 3. *In vitro* antioxidant activity of the ligands.

S. No.	Compound	% Free radical scavenging activity in different concentrations			
		0.002 μm	0.004 μm	0.006 μm	0.008 μm
1	Ascorbic acid	76.33	84.90	87.66	91.62
2	L ₁	33.33	39.00	53.66	70.66
3	L ₂	38.33	42.66	55.00	72.33

Accepted Manuscript

Table 4. *In vitro* antidiabetic activity of the ligands and complexes.

S.No.	Compound	% α -amylase inhibition
	Acarbose	97.62
1	Chromium(III) chloride	34.40
2	L ₁	38.06
3	L ₂	44.18
4	1	48.08
5	2	51.34
6	3	70.63
7	4	80.44

Accepted Manuscript

Table 5. Changes in blood glucose level (in mg/dL).

Treatment group	Blood glucose level (in mg/dL)				% GL
	0 Days	7 Days	14 Days	21 Days	
Group 1 (Control)	92.57±1.650	94.30±1.778	96.00±2.117	95.83±1.986	--
Group 2 (Stz Control)	292.73±2.868	298.03±4.206	302.77±4.245	305.40±3.780	--
Group 3 (Std)	292.63±3.050	185.20±6.022	128.27±5.845	113.57±7.694	61.18
Group 4 chromium complex (100 mg/Kg)	281.33±6.341	239.97±4.086	193.07±3.252	172.27±3.782	38.76
Group 5 chromium complex (200 mg/Kg)	265.37±8.905	222.70±6.200	176.30±4.976	154.77±5.897	41.67

Values are presented as mean ± S.E.M.; n=3 in each group. One way ANOVA followed by Dennett's, $p < 0.05$; $p < 0.01$; chromium complex, Glibenclamide (600 µg/kg body weight p.o.).

Accepted Manuscript

Table 6. *In vivo* antioxidant activity of complex 4.

Treatment group	Oxidative parameters			
	LPO (nM MDA /g wet tissue)	SOD (U/g wet tissue)	GSH (nmole/g of wet tissue)	CAT (U/g wet tissue)
Group 1 (Control)	12.44	348.50	8.81	35.31
Group 2 (Stz Control)	34.61	183.15	0.73	14.49
Group 3 (Std)	13.83	310.72	5.51	32.26
Group 4 chromium complex (100 mg/kg)	20.83	237.94	2.57	22.27
Group 5 chromium complex (200 mg/kg)	16.94	284.41	4.51	27.40

LPO -Lipid peroxidation, SOD -superoxide dismutase, GSH -reduced glutathione, CAT -catalase. n=3 animals in each group. Values are expressed as mean±SEM. Unpaired 't' test when compared with vehicle control $p < 0.001$. One way ANOVA followed by Dunnett's test when compared with Group 2 $bP < 0.05$, $cP < 0.01$, $dP < 0.001$.

Table 7. Antibacterial activity of the ligands and complexes against *E. coli*.

S. No.	Compounds	*Diameter of inhibition zone (in mm)	Minimum inhibitory concentration (in µg/mL)
1.	Standard drug Amoxicillin	49±0.04	
2.	L ₁	27±0.5	-
3.	L ₂	32±0.5	-
4.	1	34±0.6	31
5.	2	35±0.8	34
6.	3	38±0.5	37
8.	4	41±0.6	32
9.	DMSO	06±0.8	-

*Values as mean ±Standard Error Mean.

Accepted Manuscript